Journal of Colloid and Interface Science 578 (2020) 146–154

Contents lists available at ScienceDirect

Journal of Colloid and Interface Science

journal homepage: www.elsevier.com/locate/jcis

Femtosecond laser preparing patternable liquid-metal-repellent surface for flexible electronics

Jingzhou Zhang [a], Keyue Zhang [c], Jiale Yong [a], Qing Yang [b], Yongning He [c], Chengjun Zhang [b], Xun Hou [a], Feng Chen [a,*]

[a] State Key Laboratory for Manufacturing System Engineering and Shaanxi Key Laboratory of Photonics Technology for Information, School of Electronics & Information Engineering, Xi'an Jiaotong University, Xi'an 710049, PR China
[b] School of Mechanical Engineering, Xi'an Jiaotong University, Xi'an 710049, PR China
[c] School of Microelectronics, School of Electronic & Information Engineering, Xi'an Jiaotong University, 710049, PR China

GRAPHICAL ABSTRACT

A Liquid-metal-repellent surface can be achieved by femtosecond laser direct writing (FLDW). The flexibility of FLDW enables the design of colourful liquid-metal wetting/dewetting patterns by selectively treating the PDMS surface. A flexible microheater and a microstrip patch antenna were successfully prepared based on laser-textured liquid-metal-repellent surfaces.

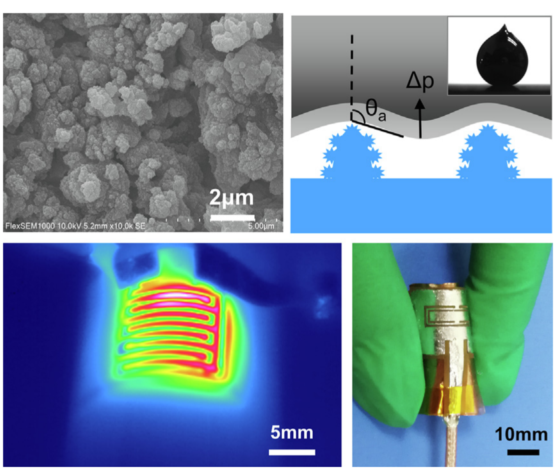

ARTICLE INFO

Article history:
Received 18 December 2019
Revised 12 May 2020
Accepted 13 May 2020
Available online 21 May 2020

Keywords:
Liquid-metal repellence
Flexible electronics

ABSTRACT

Hypothesis: Controlling the wetting behaviour of gallium-based liquid metal is highly desired for soft electronics applications. Currently, achieving durable and patternable liquid-metal-repellent surfaces by a simple and flexible method is challenging. The femtosecond laser has a remarkable ability to modify the morphology and wettability of a solid surface. It can also potentially be applied to control the wettability of liquid metal and achieve complete liquid-metal patterns.
Experiments: Femtosecond laser processing was used to form a microstructure on a polydimethylsiloxane (PDMS) surface. With regard to the laser-ablated surface, its morphology was observed by a scanning electron microscope, and its wettability to liquid metal was characterized by measuring the contact

* Corresponding author.
E-mail address: chenfeng@mail.xjtu.edu.cn (F. Chen).

https://doi.org/10.1016/j.jcis.2020.05.055

Liquid metal
Femtosecond laser
Patch antenna

angle, sliding angle, and adhesive force. Finally, its potential applications in soft electronics were demonstrated.
Findings: A layer of micro/nanostructures was directly prepared on the PDMS surface by laser ablation, presenting excellent liquid-metal repellence. Without expensive masks and complex operation processes, programmable liquid-metal-repellent patterns were easily obtained by femtosecond laser selectively treating the PDMS surface, enabling EGaIn to be patterned on the textured surface. The as-prepared liquid-metal patterns can be used as a flexible microheater and a microstrip patch antenna. It is believed that laser-patterned liquid-metal-repellent surfaces will have significant applications in soft electronics, such as antennas, microcircuits, lab on chips, and wearable electronic devices.

1. Introduction

Flexible electronics attract tremendous scientific interest because of their broad applications in portable equipment [1–3], antennas [4–6], sensors [7–9], healthcare [10–12], and wearable devices [13–16]. Outstanding stretchable and deformable components, especially flexible conductors, play a significant role in soft electronics [1,17,18]. Traditional metal conductors such as silver, copper, and aluminium have high conductivity but are not durable after repeated bending, warping, or stretching. In contrast, gallium (Ga) and Ga-based metal alloys, which are usually liquid state at room temperature, also have the advantages of strong ductility, great flexibility, and nontoxicity apart from high conductivity [19–23]. The excellent mechanical and electrical properties allow Ga-based liquid metals to become promising candidates in flexible electronics to replace traditional metal conductors [24–28]. However, liquid Ga-based metal alloys are generally coated with a thin oxide shell, and their practical application is seriously hindered by this oxide shell [29,30]. The liquid metal is inclined to firmly stick to a solid surface because the shell has ultrahigh adhesion to the solid substrate. The adhered liquid metal is difficult to remove, and the metal residuals strongly limit the precision of the preparation of Ga-based microelectronic devices. Although the unwished oxide shell can be removed by acid or alkaline solution treatment, the oxide coating will quickly regenerate through oxidation once the liquid alloys are in contact with air [31–34]. In addition, most of the acid/alkaline solutions used to remove the oxide shell are corrosive and not suitable for microelectronic devices [35].

To reduce the adhesion between liquid metal and solid surface, a new strategy based on liquid-metal-repellent microstructure is developed, without the removal of the oxide shell [36–40]. Inspired by the extremely liquid-metal-repellent surfaces that are designed by the cooperative effect of both surface microstructure and chemical composition, liquid-metal-repellent surfaces have been fabricated. For instance, Kim et al. transferred aligned carbon nanotube forest onto a polydimethylsiloxane (PDMS) surface [41]. The contact angle (CA) of a liquid galinstan® (78.3% Ga, 14.9% In, 6.8% Sn) droplet on the as-prepared surface was higher than 155°, and the CA hysteresis was 19°. Jiang et al. coated low-surface-energy silica nanoparticles onto a glass surface [42]. As a result, the glass surface was not wetted by EGaIn (85.8% Ga, 14.2% In). A complex wetting/dewetting pattern to liquid metal was further achieved by selectively and partly removing the nanoparticle coating. Joshipura et al. prepared a "never-wet" channel for EGaIn via superhydrophobic spray-coating [43]. Currently, liquid-metal repellence is usually obtained on superhydrophobic coatings, but the wettability of a Ga-based liquid-metal droplet on a rough solid substrate is very different from that of a water droplet. The influencing factor on the wettability of Ga-based liquid metal and the principle of designing a liquid-metal-repellent surface are still not deeply revealed. In addition, for application in soft microelectronic devices, wetting/dewetting micropatterned surfaces to liquid metals are strongly required in most cases. However, the reported liquid-metal-repellent patterned surfaces are usually prepared by expensive masks and complex substrates, and the fabricated liquid-metal patterns are also not durable enough in practical applications [7,17,18,44]. Achieving durable and patternable liquid-metal-repellent surfaces by a one-step and flexible approach is challenging.

Femtosecond laser direct writing (FLDW) is able to prepare various patterns on a solid surface and modify the surface topography [45–53]. Herein, micro/nanostructures were successfully built on a polydimethylsiloxane (PDMS) surface via FLDW. The droplet of EGaIn liquid metal was strongly repelled by the femtosecond laser-induced microstructures because the oxide shell makes the contact between liquid metal and the laser-induced surface microstructure be in the Cassie state. The resultant surface could maintain its liquid-metal repellence even after bending, rubbing, or immersion in different corrosive/organic solutions. Furthermore, the liquid-metal-repellent pattern was easily prepared through selective FLDW, with a metal-line resolution of 200 μm. Based on the liquid-metal-repellent patterns, soft electronics, such as microheaters and flexible microstrip patch antennas, were successfully designed.

2. Results and discussion

2.1. Topography and wettability of the laser-induced PDMS surface

FLDW is adopted to generate the microstructure on the surface of the PDMS substrate. The femtosecond laser microfabrication system is depicted in Fig. 1A. A PDMS film is fixed on a platform whose movement is controlled by the programme. The laser beam is focused onto the sample surface by an objective lens. The sample is ablated by a laser at a power of 20 mW, a scanning speed of 8 mm/s, and a scanning space of 8 μm based on a point-by-point scanning process (Fig. S1, Supporting Information). Fig. 1B, C shows scanning electron microscopy (SEM) images of the femtosecond laser-irradiated PDMS surface. Abundant micro-protrusions with sizes of 1–5 μm distribute the sample surface (Fig. 1B). The surface of the protrusions is further decorated with numerous submicro/-nanoparticles (Fig. 1C). The surface roughness (Sa) is measured to be ~0.335 μm. When a liquid EGaIn droplet controlled by a syringe needle (4 μL) is moved to touch and then leave the sample surfaces, the droplet finally adheres to the untreated flat PDMS surface firmly (Fig. 1D and Movie S1, Supporting Information), whereas the liquid-metal droplet is repelled by the laser-ablated PDMS with surface micro/nanostructures and is taken away by the syringe needle (Fig. 1E and Movie S1, Supporting Information). The liquid-metal droplet on the flat PDMS surface has a metal contact angle (MCA) of 137° ± 5° (Inset of Fig. 1F), while it can maintain a quasi-spherical shape on the laser-treated PDMS surface, and the measured MCA reaches 156.5° ± 1.5° (Inset of Fig. 1G). As the laser-structured surface is slightly tilted at 5°, the liquid-metal droplet will easily roll down (Fig. S2 and Movie S2, Supporting Infor-

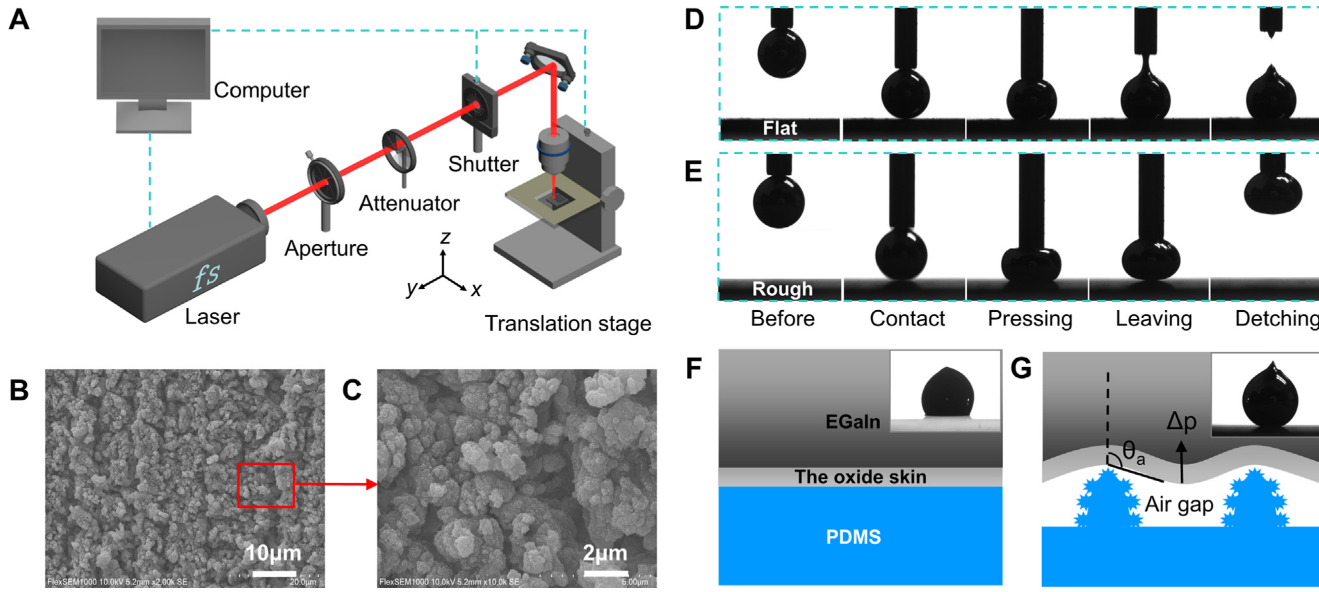

Fig. 1. Femtosecond laser microfabrication system and wettability of the PDMS surface. (A) Schematic illustration of the experimental setup. (B, C) SEM images of the PDMS surface after FLDW treatment. (D, E) Process of a liquid EGaIn droplet being moved to contact and leaving the PDMS surface: (D) the flat PDMS surface and (E) the laser-structured PDMS surface. (F, G) Schematic illustration of the wetting state between EGaIn and PDMS surfaces: (F) untreated flat PDMS surface and (G) the laser-induced rough PDMS surface. Insets: Shapes of a liquid EGaIn droplet on the corresponding surfaces.

mation). The results reveal that the laser-treated PDMS surface exhibits excellent repellence and ultralow adhesion to a liquid EGaIn droplet. We choose "liquid-metal repellence" to define the surface where a Ga-based liquid metal droplet has a CA larger than 150° and sliding angle (SA) smaller than 10° on a surface.

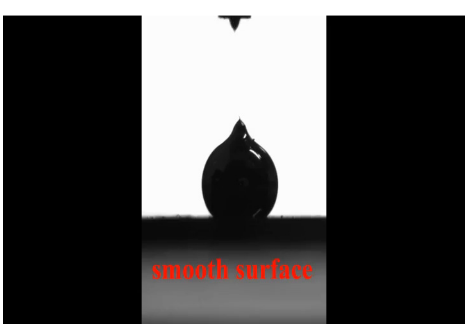

Movie S1.

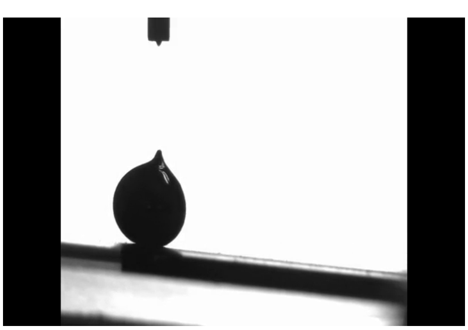

Movie S2.

As a non-Newtonian liquid, liquid EGaIn is usually coated with a solid but stretched oxide shell in an air environment. The movement of the liquid metal actually also depends on the outer oxide shell. In the case of a liquid-metal droplet on the flat PDMS surface, the PDMS surface is directly in contact with the oxide shell rather than the liquid metal (Fig. 1F). Owing to the hydrogen bond interaction between the Ga_2O_3 of the oxide layer and the hydrogen atoms of CH_3 [3,10], the large contact area between the flexible shell and PDMS surface leads to ultrahigh adhesion of the untreated PDMS surface to the liquid metal.

When liquid metal is in contact with the femtosecond laser-structured surface, the oxide shell first touches the microprotrusions and nanoparticles on the sample surface, as shown in Fig. 1G. The limit of the intrusion pressure, Δp, can be illustrated as:

$$\Delta p = -\frac{\gamma L \cos\theta_a}{S}$$

where γ is the surface tension of the oxide shell ($\gamma \approx 600$ mN/m), L is the length of the three-phase (air/solid/liquid metal) contact line, θ_a is the advancing CA, and S is the projected contact area. The γ of the EGaIn oxide shell is much larger than the surface tension of common liquids such as water and oil. The θ_a of EGaIn is also greater than that of water on the PDMS surface. Hence, compared to common Newtonian liquids, Ga-based liquid metal is more difficult to wet rough surfaces. To further analyse the similarity and difference between water and EGaIn wetting behaviours, the influences of physical morphology and chemical composition are discussed in detail in the Supporting Information. The wettability of Ga-based liquid metal is very different from the water wettability. The laser-induced hydrophilic microstructure can also have liquid-metal repellent ability in addition to a superhydrophobic surface. Fig. S3 (Supporting Information) reveals that the surface microstructure plays a more important role in achieving liquid-metal repellence than chemistry. Therefore, liquid-metal repellence is proven to be simply achieved via FLDW, regardless of chemical modification.

The average distance (AD) of the laser pulse-ablated points has a great influence on the surface morphology of the laser-treated PDMS surface (Fig. S1, Supporting Information). Fig. 2A–C shows the SEM images of the laser-structured PDMS surfaces with differ-

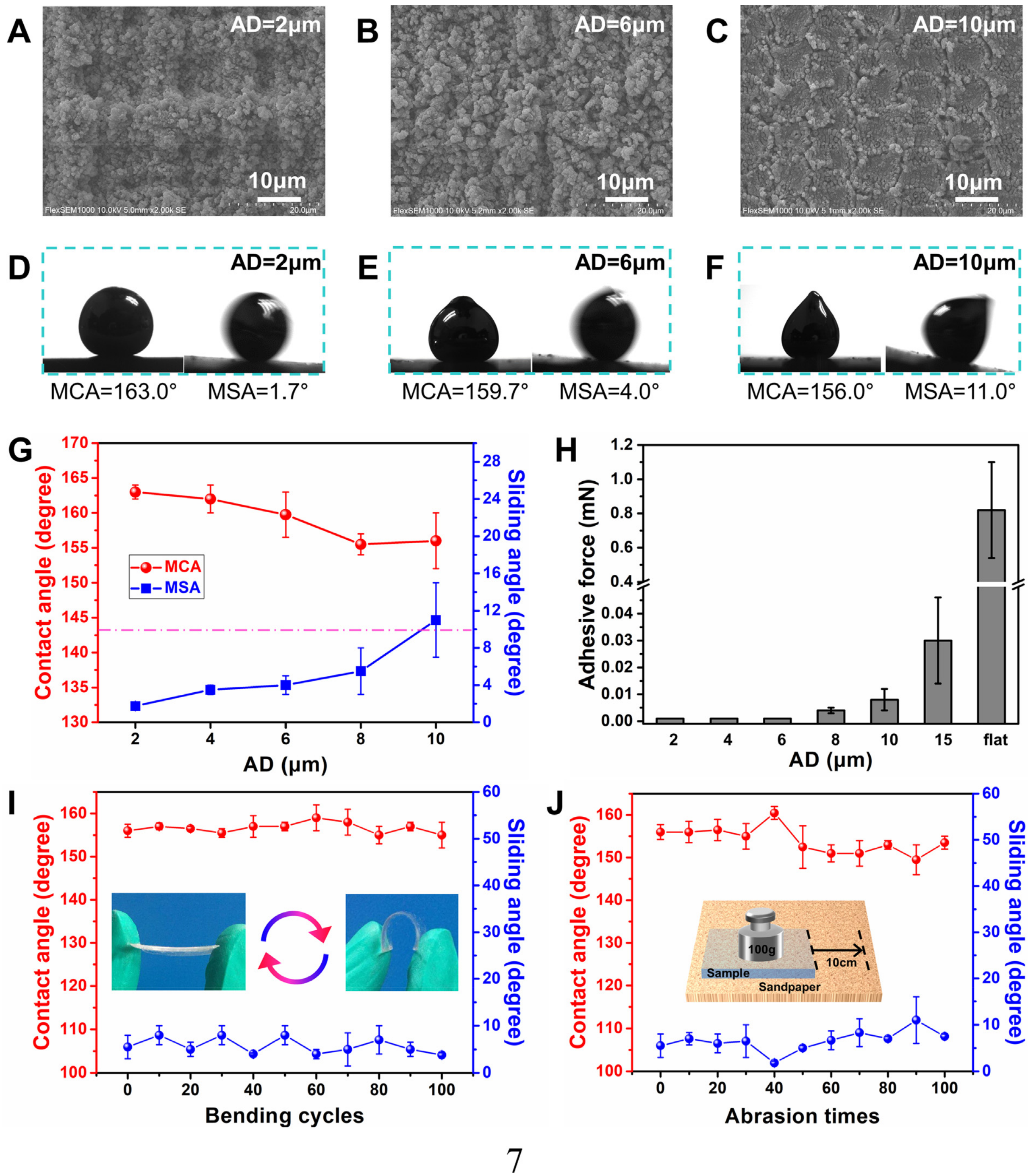

Fig. 2. SEM images of the PDMS surface after FLDW treatment: (A) AD = 2 μm, (B) AD = 6 μm, and (C) AD = 10 μm. (D–F) Static shape and sliding behaviour of a liquid EGaIn droplet on the resultant surfaces corresponding to (A–C). (G) Variation of the MCA and MSA of the laser-irradiated PDMS surface with the change of the AD. (H) Adhesive force between the EGaIn droplet and the laser-irradiated PDMS surfaces with different ADs. (I, J) The MCA and MSA on the laser-treated surface after the (I) bending test and (J) abrasion test.

ent ADs. The amount of microstructures and nanostructures on the resultant surface decreases with increasing AD. The *Sa* decreases from 0.445 μm to 0.12 μm as the AD increases from 2 μm to 15 μm (Fig. S4, Supporting Information). The variation of surface microstructures results in the change of EGaIn wetting behaviour on the resultant surface. Fig. 2G shows the MCAs and metal sliding angles (MSAs) on the sample surfaces with the AD ranging from 2 μm to 10 μm. The MCA is as high as 163.0° ± 1°, and the MSA is only 1.7° ± 0.3° at an AD of 2 μm (Fig. 2D). As the AD increases, the MCA slowly decreases from 163.0° ± 1° (AD = 2 μm) to 162.0° ± 2° (AD = 4 μm), 159.7° ± 3.3° (AD = 6 μm, Fig. 2E), 155.5° ± 1.5° (AD = 8 μm) and then to 156.0° ± 4° (AD = 10 μm, Fig. 2F). In contrast, the MSA slowly increases as the AD increases. The MSA is larger than 10° until the AD reaches up to 10 μm (Fig. 2E–G). The adhesive force between a liquid EGaIn droplet and the laser-structured PDMS surface is revealed in Fig. 2H. The variation trend of the adhesive force is similar to that of the MSA. The adhesive force is smaller than 0.003 mN when the AD is less than 8 μm. Compared to the flat PDMS surface, the adhesive force between EGaIn liquid metal and PDMS surface is reduced at least 266 times after FLDW treatment. Therefore, a liquid-metal-repellent surface with ultralow metal adhesion can be obtained with an AD less than 8 μm.

2.2. Durability of liquid-metal-repellent surface

Mechanical and chemical durability (e.g., anti-abrasion, bendable, and anti-corrosion) is crucial for liquid-metal-repellent surfaces for practical applications. Most of the pre-reported liquid-metal-repellent surfaces are fabricated by coating rough micro/nanostructures on a substrate. The surfaces are easy to lose liquid-metal-repellent properties as long as the coatings are broken or peeled off. In contrast, femtosecond laser-structured surfaces exhibit stable liquid-metal repellence after different damage treatments. Fig. 2I shows the metal wettability of the laser-structured PDMS surface after being bent to a significant degree for different cycles. The MCA and MSA show almost no apparent change after 100 bending cycles. As shown in Fig. 2J, a simple sandpaper abrasion test was also performed to investigate the wear resistance of the laser-induced microstructures. With increasing abrasion time, the MCA of a liquid metal droplet on the treated PDMS surface is always larger than 150°, and the MSA is kept below 10°. Moreover, the sample still maintained great liquid-metal repellence after immersion in 1 M HCl, 1 M NaOH, 10 wt% NaCl, and 10 wt% glucose solutions for 4 h (Fig. S5, Supporting Information). The results demonstrate that the laser-induced liquid-metal-repellent surface possesses strong mechanical robustness and chemical stability.

The femtosecond laser pulse is able to ablate almost all of the solid materials due to its extremely high peak intensity, so FLDW can endow various materials with rough surface microstructures apart from the PDMS film. After the formation of surface

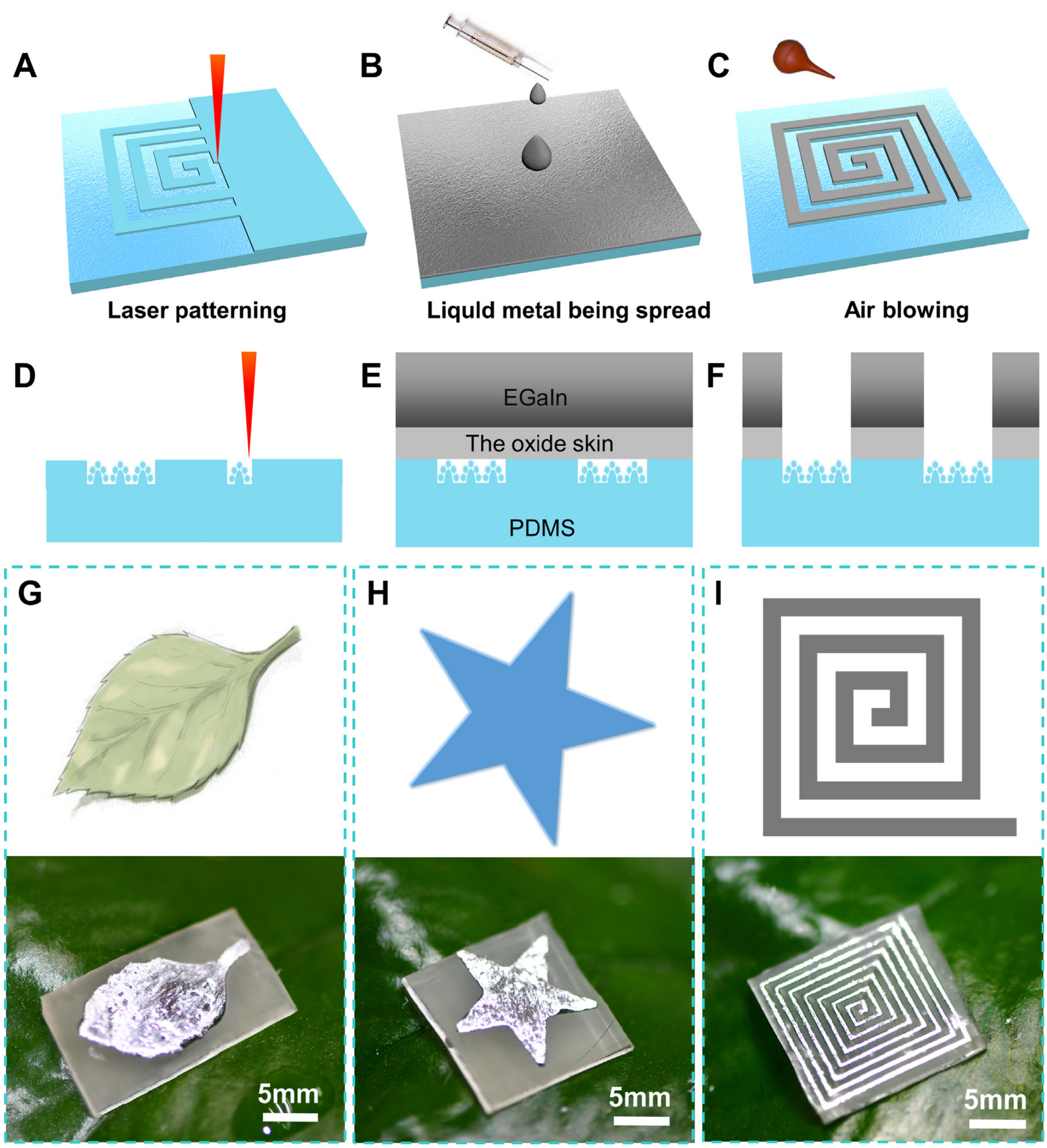

Fig. 3. Fabrication of liquid-metal patterns by selective FLDW. (A–C) Process of preparing a liquid-metal pattern by FLDW: (A) patterning the PDMS surface by selective laser treatment, (B) dripping liquid metal onto the patterned surface, (C) air blowing. (D–F) Schematic illustration of the wetting state between liquid metal and the PDMS surface corresponding to (A–C). (G–I) Photos of the liquid-metal patterns with different shapes: (G) leaf-like pattern, (H) star-like pattern, and (I) complex spiral pattern.

microstructures by FLDW, the laser-structured Cu, Ti, glass, and Si surfaces also present great EGaIn-repellent ability, as shown in Fig. S6 (Supporting Information).

2.3. Fabrication of liquid metal patterns

Based on the distinguishing wettabilities of the untreated surface and laser-structured PDMS surface, EGaIn patterns can be designed and fabricated via selective FLDW, as shown in Fig. 3A–F. First, part of the PDMS surface area was selectively ablated by a femtosecond laser, leaving the rest of the region composed of an unablated flat area (Fig. 3A, D). The unablated flat area formed a pattern whose shape can be predesigned by a computer programme during laser treatment. Second, liquid EGaIn was dripped onto the patterned surface and brushed over the whole surface to entirely spread it out (Fig. 3B). As shown in Fig. 3E, the oxide shell of EGaIn only wetted the unablated flat area, belonging to Young's contact state. However, the contact between the oxide shell and laser-irradiated area was prevented by microprotrusions and nanoparticles. The EGaIn oxide shell can only touch the peaks of the micro/nanostructures of the laser-ablated area, reducing the real contact area between the oxide shell and the rough structures remarkably. Such solid/solid (rough surface/oxide shell) contact can be considered as the Cassie contact state. Third, the excess liquid metal on the sample surface was simply removed by air blowing (Fig. 3E). Due to the different contact states between the oxide shell and laser-ablated/unable-ablated area, liquid metal on the rough area was easily removed by air blowing, and the liquid EGaIn only adhered on the flat area (Fig. 3F). Finally, the surface was brushed again to uniformize the EGaIn layer. As a result, an EGaIn metal pattern based on the surface structure pattern was obtained (Fig. 3C). Through designing different structural patterns on the PDMS surface by selective FLDW, complex metal micropatterns can be successfully prepared, such as leaf-like patterns (Fig. 3G), star-like patterns (Fig. 3H), and circuit patterns (Fig. 3I). The thickness of the liquid metal pattern is approximately 10 μm. The excellent electrical and mechanical properties allow the designed EGaIn patterns to be applied in microelectronics. Fig. S7A (Supporting Information) shows a simple circuit with a line width of 500 μm, which is highly uniform. The line width of EGaIn can be easily tuned by the designed pattern, and a minimum line width of 200 μm can be achieved (Fig. S7B, Supporting Information).

2.4. Application of patternable liquid-metal-repellent surface

2.4.1. Microheater

A microheater based on a patterned liquid-metal-repellent surface was designed. The layout of the circuit is depicted in Fig. 4A. The width of the as-prepared liquid metal line is 1000 μm and the resistance of the circuit remains stable at 1.2 Ω. When an input current is applied to the as-prepared circuit, the EGaIn-based device is able to generate heat. Fig. 4B shows the infrared temper-

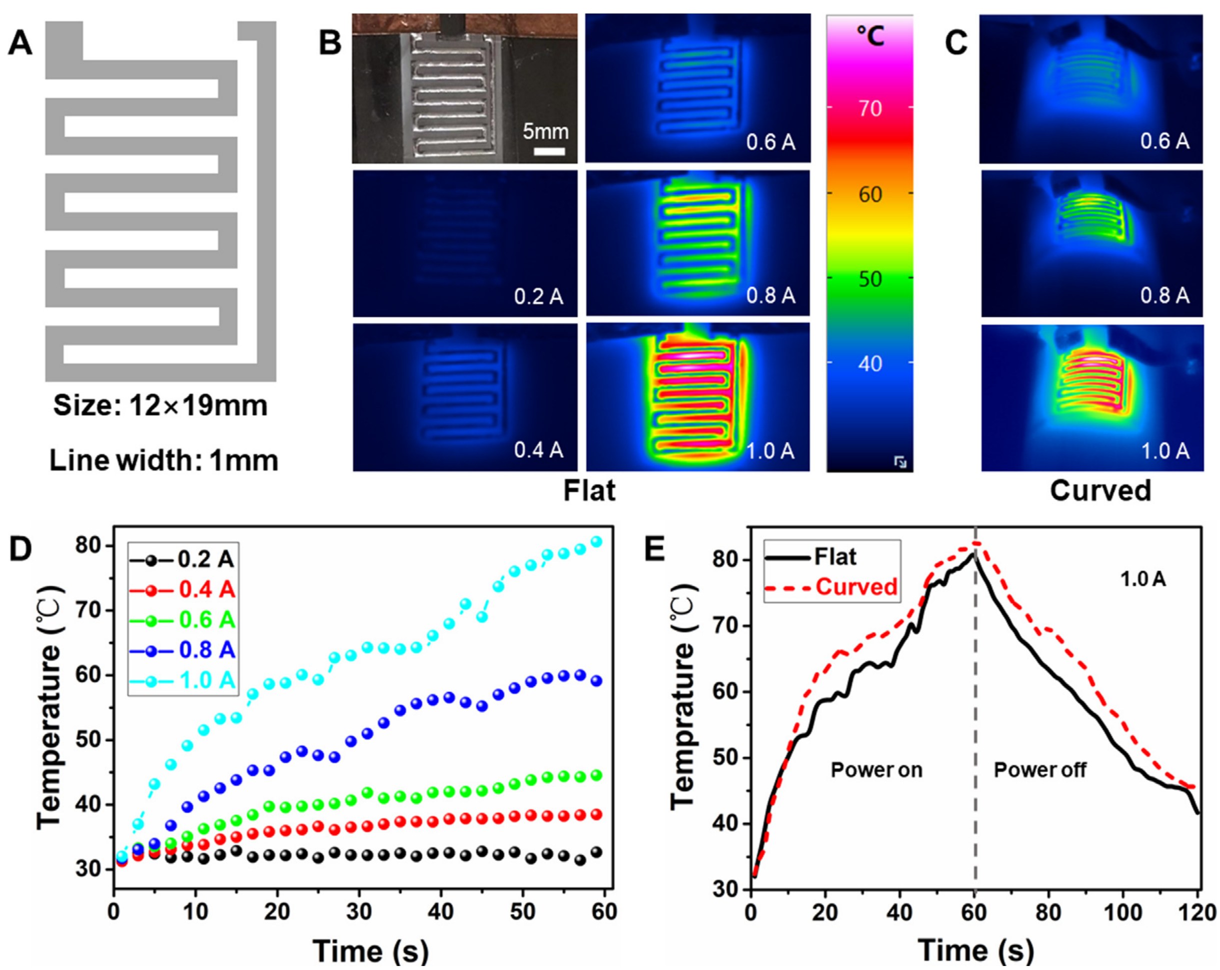

Fig. 4. Microheater based on an EGaIn pattern. (A) Design diagram of the microheater. (B, C) Photo of the as-prepared micro-heater and its infrared temperature distribution images under different input currents: (B) the flat microheater and (C) the curved microheater. (D) Temperature of the microheater after applying different currents for 0–60 s. (E) Temperature evolutions of the microheater at the flat and curved states during a cycle of heating and cooling down (I = 1.0 A).

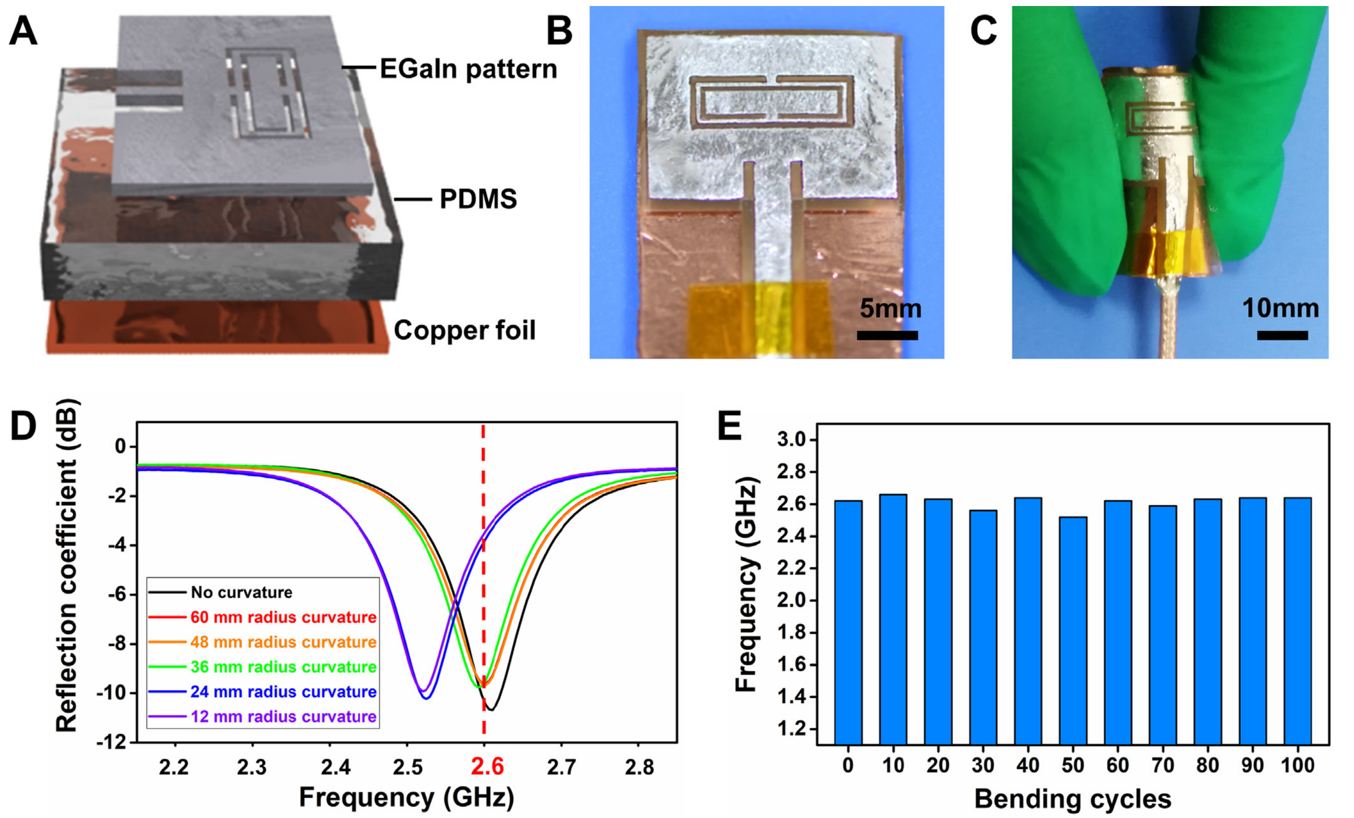

Fig. 5. Flexible microstrip patch antenna based on an EGaIn pattern. (A) Component of the patch antenna. (B, C) Photos of the (B) flat and (C) curved patch antennas. (D) Measured frequency of the as-prepared patch antenna with different bending conditions. (E) Dependence of the working frequency on the bending cycles of the antenna.

ature distribution images of the circuit after being applied with different input currents for 60 s. The heat-generation results are summarized in Fig. 4D, which is consistent with the Joule law and heat dissipation. With increasing time, the temperature of the as-prepared device gradually increases at first and finally stabilizes. The input current plays an important role in the heating efficiency of the microheater as well as the maximum temperature. There is no significant temperature change between the microheater and environment when the working current is only 0.2 A. The device can be heated to 38.4 °C in the case of I = 0.4 A. It is also found that the maximum temperature of the microheater has an obviously positive correlation with the input current. As the working current further increases, the temperature can reach up to 44.6 °C (I = 0.6 A), 60.0 °C (I = 0.8 A) and 81.0 °C (I = 1.0 A), as shown in Fig. 4B. Even though the microheater was bent, it was still able to generate heat (Fig. 4C). Fig. 4E shows the temperature evolutions of the microheater at the flat and curved states during a cycle of heating and cooling down (I = 1.0 A). The temperature variation trend of the curved microheater almost coincides with that of the flat microheater, indicating that the as-prepared microheater can even continue to work entirely with a bent shape. The capacity of working at the curved state of the as-prepared microheater is ascribed to the strong ductility and great flexibility of the Ga-based liquid metal.

2.4.2. Microstrip patch antenna

A flexible microstrip patch antenna was also prepared based on the EGaIn pattern. As shown in Fig. 5A, the patch antenna consists of an EGaIn pattern, a PDMS layer, and a copper foil. EGaIn was adhered on the patterned liquid-metal-repellent PDMS layer as the metal patch of the antenna. Copper foil tape was pasted under PDMS. The whole antenna has a size of 20×23 mm^2, and the minimum line width of the EGaIn pattern is only 300 μm (Fig. 5B). No surprisingly, the designed working frequency is 2.6 GHz according to the simulation. The experimental results reveal that the as-prepared microstrip patch antenna works only at 2.6 GHz, agreeing well with the design requirement (Fig. 5D). When the antenna is bent from flat to a curved surface with a radius curvature of 36 mm (Fig. 5C), the resultant antenna always works at 2.6 GHz, and no significant shift of working frequency occurs. As the radius of curvature decreases to 24 mm, the centre frequency of the resultant antenna has a slight decrease, and this shift is no more than 0.1 GHz. Generally, such subtle fluctuation of the centre frequency is in the normal working range. Fig. 5D also reveals that all the curved antennas with different radius curvatures present good input matching and work near 2.6 GHz, demonstrating the excellent flexibility and ductility of the as-obtained antenna. The flexible microstrip patch antenna is still able to work properly after 100 cycles of bending treatment (Fig. 5E). The features of good input matching and flexibility allow the EGaIn-based antenna to have broad commercial application prospects in soft electronic devices.

3. Conclusions

In conclusion, a novel way to prepare liquid-metal-repellent surfaces was realized by a femtosecond laser. The laser-induced micro/nanoscale surface structure endowed the PDMS surface with excellent repellence to liquid metal. On the resultant surface, the adhesive force between the liquid metal and the textured surface was reduced by at least 266 times compared to untreated flat PDMS. It is also revealed that the wettability of Ga-based liquid metal is very different from the water wettability. Surface microstructure plays a more important role than chemistry in achieving liquid-metal repellence. The resultant surface could maintain its liquid-metal-repellent property even after bending, rubbing, or immersion in different corrosive/organic solutions, which presents unique stability compared with that of other liquid-metal-repellent surfaces [41–43]. The flexibility of FLDW enables the design of colourful liquid-metal wetting/dewetting patterns by selectively treating the PDMS surface. The as-prepared liquid-metal patterns can be used as a flexible micro-heater and a flexible patch antenna. The minimum metal-line width of 200 μm is obtained. Furthermore, the whole liquid metal pattern is directly formed on a single micro/nanostructured substrate that is pretreated by a femtosecond laser. Compared to the existing technology for printing liquid metal, this selective liquid metal wetting process is very simple and flexible and does not require any masks, coatings, or extra equipment [17,18,44].

This concept will open a new way to print soft electronics by just controlling the physical morphology of the substrate surface. Further studies are important to improve the machining precision and miniaturize the devices. It is believed that laser-patterned liquid-metal-repellent surfaces will have more significant applications in liquid metal printing, microfluidics, soft robots, and wearable devices.

4. Experimental section

4.1. Materials

PDMS is a kind of soft, transparent, and eco-friendly polymer that is widely used in flexible and wearable electronics. The PDMS sheets were prepared from a 1:10 mixture of curing agent (DC-184B, Dow Corning Corporation) and prepolymer (DC-184A, Dow Corning Corporation). The PDMS mixture was cured at 90 °C for 2 h. The EGaIn (85% Ga & 15% In) liquid metal was purchased from Shuochen Metal Co., Ltd.

4.2. FLDW process

As shown in Fig. 1A, PDMS sheets with a thickness of 0.5 mm were mounted on a computer-controlled translation stage. The laser pulses (centre wavelength = 800 nm, pulse duration = 50 fs, repetition rate = 1 kHz) were generated from a regenerative amplified Ti:sapphire laser system (CoHerent, Libra-usp-1 K-he-200) and were focused onto the sample surfaces by an objective lens (20×, NA = 0.45). The laser power was set at 20 mW. During femtosecond processing, the laser scanning speed and the interval of the scanning lines were controlled by the programme. The average distance (AD) of the adjacent laser-ablated points is the main machining parameter in our experiment (Fig. S1, Supporting Information). After that, the samples were cleaned by an ultrasonic cleaner.

4.3. Fabrication of flexible antenna

The antenna was designed and simulated in commercially available 3D electromagnetic software, CST. According to the metal patch of an antenna, the EGaIn pattern was achieved on the PDMS surface by selective FLDW. A copper foil tape was cut to the right dimension and then pasted under the PDMS surface. To ensure electrical connection at the feeding port, thin cable and antenna with high temperature resistant insulation tape were fixed. The as-obtained antenna has a size of 20×23 mm^2, and the connector is attached from the bottom side.

4.4. Characterization

A Flex SEM 1000 scanning electron microscope (HITACHI, Japan) was used to observe the morphology of the as-prepared surface. The three-dimensional profile and surface roughness of the PDMS surface were examined by a LEXT OLS4000 laser confocal microscope (Olympus, Japan). The EGaIn and water contact angles and sliding angles were measured by a JC2000D contact-angle system (Powereach, China). The volume of the tested droplet was approximately 8 μL. The dynamic process of EGaIn droplets was captured by a charge-coupled device camera with a frame rate of 100 fps. The adhesive force between a liquid-metal droplet and the untreated/treated surfaces was measured using a DCAT 11 surface tension measurement system (Dataphysics, Germany). The infrared temperature distribution of the EGaIn-based microheater was measured by a VarioCAM-780 infrared thermal imager (InfraTec, Germany). The frequency of the antenna was characterized with a Rhode and Schwarz ZVR vector network analyzer.

4.5. Durability test

For the sandpaper abrasion test, the laser-structured PDMS sample (2×2 cm^2) was placed on sandpaper (1000 mesh, Sail Brand, China) and the laser-treated side was in contact with the sandpaper. The PDMS sample also loaded a weight of 100 g. Every time the surface was pulled forward for 10 cm and then returned back. The bending test was carried out by curving the sample to 180° for different cycles. The chemical durability was evaluated by immersing the sample in different solutions for 4 h, including 0.01 mol/L hydrochloric acid, 0.01 mol/L sodium hydroxide, 10% sodium chloride, and 10% glucose solutions.

CRediT authorship contribution statement

Jingzhou Zhang: Conceptualization, Methodology, Data curation, Formal analysis, Writing - original draft. **Keyue Zhang:** Software. **Jiale Yong:** Supervision, Writing - review & editing. **Qing Yang:** Supervision. **Yongning He:** Supervision. **Chengjun Zhang:** Validation. **Xun Hou:** Supervision. **Feng Chen:** Project administration, Writing - review & editing.

Acknowledgements

This work is supported by the National Science Foundation of China under the Grant nos. 61875158, U1630111 and 61435005, the National Key Research and Development Program of China under the Grant no.2017YFB1104700, the Fundamental Research Funds for the Central Universities, the International Joint Research Laboratory for Micro/Nano Manufacturing and Measurement Technologies, Instrument Analysis Center of Xi'an Jiaotong University.

Appendix A. Supplementary data

Supplementary data to this article can be found online at https://doi.org/10.1016/j.jcis.2020.05.055.

References

[1] M.G. Mohammed, R. Kramer, All-printed flexible and stretchable electronics, Adv. Mater. 29 (2017) 1404965.
[2] G. Li, M. Parmar, D.W. Lee, An oxidized liquid metal-based microfluidic platform for tunable electronic device applications, Lab Chip 15 (2015) 766–775.
[3] T. Daeneke, K. Khoshmanesh, N. Mahmood, I.A. de Castro, D. Esrafilzadeh, S.J. Barrow, M.D. Dickey, K. Kalantar-Zadeh, Liquid metals: fundamentals and applications in chemistry, Chem. Soc. Rev. 47 (2018) 4073–4111.

[4] M. Wang, C. Trlica, M.R. Khan, M.D. Dickey, J.J. Adams, A reconfigurable liquid metal antenna driven by electrochemically controlled capillarity, J. Appl. Phys. 117 (2015) 194901.
[5] Y. Damgaci, B.A. Cetiner, A frequency reconfigurable antenna based on digital microfluidics, Lab Chip 13 (2013) 2883–2887.
[6] J. Trajkovikj, J.F. Zurcher, A.K. Skrivervik, Soft and flexible antennas on permittivity adjustable PDMS substrates, 2012 Loughborough Antennas & Propagation Conference (Lapc) (2012).
[7] R.K. Kramer, C. Majidi, R.J. Wood, Masked deposition of Gallium-Indium alloys for liquid-embedded elastomer conductors, Adv. Funct. Mater. 23 (2013) 5292–5296.
[8] T. Yang, B. Kwon, P.B. Weisensee, J.G. Kang, X. Li, P. Braun, N. Miljkovic, W.P. King, Millimeter-scale liquid metal droplet thermal switch, Appl. Phys. Lett. 112 (2018) 063505.
[9] R. Rahimi, M. Ochoa, B. Ziaie, Comparison of direct and indirect laser ablation of metallized paper for inexpensive paper-based sensors, ACS Appl. Mater. Interfaces 10 (2018) 36332–36341.
[10] R. Guo, J. Tang, S. Dong, J. Lin, H. Wang, J. Liu, W. Rao, Flexible electronics: one-step liquid metal transfer printing: toward fabrication of flexible electronics on wide range of substrates, Adv. Mater. Tech. 3 (2018) 1800265.
[11] R. Guo, X. Wang, H. Chang, W. Yu, S. Liang, W. Rao, J. Liu, Ni-GaIn amalgams enabled rapid and customizable fabrication of wearable and wireless healthcare electronics, Adv. Eng. Mater. 20 (2018) 1800054.
[12] A. Hirsch, L. Dejace, H.O. Michaud, S.P. Lacour, Harnessing the rheological properties of liquid metals to shape soft electronic conductors for wearable applications, Acc. Chem. Res. 52 (2019) 534–544.
[13] M. Kubo, X. Li, C. Kim, M. Hashimoto, B.J. Wiley, D. Ham, G.M. Whitesides, Stretchable microfluidic radiofrequency antennas, Adv. Mater. 22 (2010) 2749–2752.
[14] J.J. Adams, E.B. Duoss, T.F. Malkowski, M.J. Motala, B.Y. Ahn, R.G. Nuzzo, J.T. Bernhard, J.A. Lewis, Conformal printing of electrically small antennas on three-dimensional surfaces, Adv. Mater. 23 (2011) 1335–1340.
[15] M.H. Malakooti, N. Kazem, J. Yan, C. Pan, E.J. Markvicka, K. Matyjaszewski, C. Majidi, Liquid metal supercooling for low-temperature thermoelectric wearables, Adv. Funct. Mater. 45 (2019) 1906098.
[16] N. Kazem, M.D. Bartlett, C. Majidi, Extreme toughening of soft materials with liquid metal, Adv. Mater. 30 (2018) 1706594.
[17] B.J. Carey, J.Z. Ou, R.M. Clark, K.J. Berean, A. Zavabeti, A.S. Chesman, S.P. Russo, D.W. Lau, Z.Q. Xu, Q. Bao, O. Kevehei, B.C. Gibson, M.D. Dickey, R.B. Kaner, T. Daeneke, K. Kalantar-Zadeh, Wafer-scale two-dimensional semiconductors from printed oxide skin of liquid metals, Nat. Commun. 8 (2017) 14482.
[18] T. Lu, L. Finkenauer, J. Wissman, C. Majidi, Rapid prototyping for soft-matter electronics, Adv. Funct. Mater. 24 (2014) 3351–3356.
[19] T. Liu, P. Sen, C.-J. Kim, Characterization of nontoxic liquid-metal alloy Galinstan for applications in microdevices, J. Microelectromech. Sci. 21 (2012) 443–450.
[20] Y.-H. Wu, S.-T. Xing, R.-M. Zheng, S.-Q. Liu, Z.-F. Deng, H.-Z. Liu, P.-P. Wang, L. Liu, Interface design for enhancing the wettability of liquid metal to polyacrylate for intrinsically soft electronics, J. Mater. Chem. C 6 (2018) 6755–6763.
[21] J. Wang, G. Cai, S. Li, D. Gao, J. Xiong, P.S. Lee, Printable superelastic conductors with extreme stretchability and robust cycling endurance enabled by liquid-metal particles, Adv. Mater. 30 (2018) 1706157.
[22] C. Thrasher, Z. Farrell, N. Morris, C. Willey, C. Tabor, Mechanoresponsive polymerized liquid metal networks, Adv. Mater. 31 (2019) 1903864.
[23] M.D. Dickey, R.C. Chiechi, R.J. Larsen, E.A. Weiss, D.A. Weitz, G.M. Whitesides, Eutectic Gallium-Indium (EGaIn): a liquid metal alloy for the formation of stable structures in microchannels at room temperature, Adv. Funct. Mater. 18 (2008) 1097–1104.
[24] P. Zhang, Q. Wang, R. Guo, M. Zhang, S. Wang, C. Lu, M. Xue, J. Fan, Z. He, W. Rao, Self-assembled ultrathin film of CNC/PVA-liquid metal composite as a multifunctional Janus material, Mater. Horiz. 6 (2019) 1643–1653.
[25] R. Guo, X. Sun, B. Yuan, H. Wang, J. Liu, Magnetic liquid metal (Fe-EGaIn) based multifunctional electronics for remote self-healing materials, degradable electronics, and thermal transfer printing, Adv. Sci. 6 (2019) 1901478.
[26] S. Chen, H.-Z. Wang, X.-Y. Sun, Q. Wang, X.-J. Wang, L.-B. Chen, L.-J. Zhang, R. Guo, J. Liu, Generalized way to make temperature tunable conductor–insulator transition liquid metal composites in a diverse range, Mater. Horiz. 6 (2019) 1854–1861.
[27] N. Kazem, T. Hellebrekers, C. Majidi, Soft multifunctional composites and emulsions with liquid metals, Adv. Mater. 29 (2017) 1605985.
[28] M.D. Dickey, Stretchable and soft electronics using liquid metals, Adv. Mater. 29 (2017) 1606425.
[29] R.K. Kramer, J.W. Boley, H.A. Stone, J.C. Weaver, R.J. Wood, Effect of microtextured surface topography on the wetting behavior of eutectic gallium-indium alloys, Langmuir 30 (2014) 533–539.
[30] K. Doudrick, S. Liu, E.M. Mutunga, K.L. Klein, V. Damle, K.K. Varanasi, K. Rykaczewski, Different shades of oxide: from nanoscale wetting mechanisms to contact printing of gallium-based liquid metals, Langmuir 30 (2014) 6867–6877.
[31] R.A. Bilodeau, D.Y. Zemlyanov, R.K. Kramer, Liquid metal switches for environmentally responsive electronics, Adv. Mater. Interfaces 4 (2017) 1600913.
[32] S. Holcomb, M. Brothers, A. Diebold, W. Thatcher, D. Mast, C. Tabor, J. Heikenfeld, Oxide-free actuation of Gallium liquid metal alloys enabled by novel acidified siloxane oils, Langmuir 32 (2016) 12656–12663.
[33] A.F. Chrimes, K.J. Berean, A. Mitchell, G. Rosengarten, K. Kalantar-zadeh, Controlled electrochemical deformation of liquid-phase Gallium, ACS Appl. Mater. Interfaces 8 (2016) 3833–3839.
[34] D. Kim, Y. Lee, D.-W. Lee, W. Choi, K. Yoo, J.-B. Lee, Hydrochloric acid-impregnated paper for gallium-based liquid metal microfluidics, Sensor. Actuat. B-Chem. 207 (2015) 199–205.
[35] D. Kim, P. Thissen, G. Viner, D.W. Lee, W. Choi, Y.J. Chabal, J.B. Lee, Recovery of nonwetting characteristics by surface modification of gallium-based liquid metal droplets using hydrochloric acid vapor, ACS Appl. Mater. Interfaces 5 (2013) 179–185.
[36] Y. Chen, T. Zhou, Y. Li, L. Zhu, S. Handschuh-Wang, D. Zhu, X. Zhou, Z. Liu, T. Gan, X. Zhou, Robust fabrication of nonstick, noncorrosive, conductive graphene-coated liquid metal droplets for droplet-based, floating electrodes, Adv. Funct. Mater. 28 (2018) 1706277.
[37] V. Sivan, S.-Y. Tang, A.P. O'Mullane, P. Petersen, N. Eshtiaghi, K. Kalantar-zadeh, A. Mitchell, Liquid metal marbles, Adv. Funct. Mater. 23 (2013) 144–152.
[38] S. Hammouti, B. Holybee, M. Christenson, M. Szott, K. Kalathiparambil, S. Stemmley, B. Jurczyk, D.N. Ruzic, Wetting of liquid lithium on fusion-relevant materials microtextured by femtosecond laser exposure, J. Nucl. Mater. 508 (2018) 237–248.
[39] S.S. Kadlaskar, J.H. Yoo, J.B. Abhijeet, W. Choi Lee, Cost-effective surface modification for Galinstan(R) lyophobicity, J. Colloid Interface Sci. 492 (2017) 33–40.
[40] N. Ilyas, A. Cook, C.E. Tabor, Designing liquid metal interfaces to enable next generation flexible and reconfigurable electronics, Adv. Mater. Interfaces 4 (2017) 1700141.
[41] D. Kim, D. Jung, J.H. Yoo, Y. Lee, W. Choi, G.S. Lee, K. Yoo, J.-B. Lee, Stretchable and bendable carbon nanotube on PDMS super-lyophobic sheet for liquid metal manipulation, J. Micromech. Microeng. 24 (2014) 055018.
[42] Y. Jiang, S. Su, H. Peng, H. Sing Kwok, X. Zhou, S. Chen, Selective wetting/dewetting for controllable patterning of liquid metal electrodes for all-printed device application, J. Mater. Chem. C 5 (2017) 12378–12383.
[43] I.D. Joshipura, H.R. Ayers, G.A. Castillo, C. Ladd, C.E. Tabor, J.J. Adams, M.D. Dickey, Patterning and reversible actuation of liquid Gallium alloys by preventing adhesion on rough surfaces, ACS Appl. Mater. Interfaces 10 (2018) 44686–44695.
[44] S. Zhang, B. Wang, J. Jiang, K. Wu, C. Guo, Z. Wu, High-fidelity conformal printing of 3D liquid alloy circuits for soft electronics, ACS Appl. Mater. Interfaces 11 (2019) 7184–17156.
[45] J. Zhang, J. Yong, Q. Yang, F. Chen, X. Hou, Femtosecond laser-induced underwater superoleophobic surfaces with reversible pH-responsive wettability, Langmuir 35 (2019) 3295–3301.
[46] B. Deng, G.J. Cheng, Pulsed laser modulated shock transition from liquid metal nanoparticles to mechanically and thermally robust solid-liquid patterns, Adv. Mater. 31 (2019) 1807811.
[47] J. Yong, Y. Fang, F. Chen, J. Huo, Q. Yang, H. Bian, G. Du, X. Hou, Femtosecond laser ablated durable superhydrophobic PTFE films with micro-through-holes for oil/water separation: separating oil from water and corrosive solutions, Appl. Surf. Sci. 389 (2016) 1148–1155.
[48] J. Yong, Q. Yang, F. Chen, D. Zhang, U. Farooq, G. Du, X. Hou, A simple way to achieve superhydrophobicity, controllable water adhesion, anisotropic sliding, and anisotropic wetting based on femtosecond-laser-induced line-patterned surfaces, J. Mater. Chem. A 2 (2014) 5499–5507.
[49] J. Yong, F. Chen, Q. Yang, D. Zhang, U. Farooq, G. Du, X. Hou, Bioinspired underwater superoleophobic surface with ultralow oil-adhesion achieved by femtosecond laser microfabrication, J. Mater. Chem. A 2 (2014) 8790–8795.
[50] T. Baldacchini, J.E. Carey, M. Zhou, E. Mazur, Superhydrophobic surfaces prepared by microstructuring of silicon using a femtosecond laser, Langmuir 22 (2006) 4917–4929.
[51] V. Zorba, E. Stratakis, M. Barberoglou, E. Spanakis, P. Tzanetakis, S.H. Anastasiadis, C. Fotakis, Biomimetic artificial surfaces quantitatively reproduce the water repellency of a Lotus Leaf, Adv. Mater. 20 (2008) 4049–4054.
[52] Y. Hu, Z. Wang, D. Jin, C. Zhang, R. Sun, Z. Li, K. Hu, J. Ni, Z. Cai, D. Pan, X. Wang, W. Zhu, J. Li, D. Wu, L. Zhang, J. Chu, Botanical-inspired 4D printing of hydrogel at the microscale, Adv. Funct. Mater. 30 (2020) 1907377.
[53] Z. Lao, Y. Zheng, Y. Dai, Y. Hu, J. Ni, S. Ji, Z. Cai, Z.J. Smith, J. Li, L. Zhang, D. Wu, J. Chu, Nanogap plasmonic structures fabricated by switchable capillary-force driven selfassembly for localized sensing of anti-cancer medicines with microfluidic SERS, Adv. Func. Mater. (2020) 1909467.